Solar Phys (2020) 295:73
https://doi.org/10.1007/s11207-020-01632-0

Inferring the Magnetic Field Asymmetry of Solar Flares from the Degree of Polarisation at Millimetre Wavelengths

D.F. Silva[1] · P.J.A. Simões[1,2] · R.F. Hidalgo Ramírez[1] · A. Válio[1]

Received: 5 December 2019 / Accepted: 28 April 2020 / Published online: 4 June 2020

Abstract Polarisation measurements of solar flares at millimetre-waves were used to investigate the magnetic field configuration of the emitting sources. We analyse two solar flares (SOL2013-02-17 and SOL2013-11-05) observed by the POlarisation Emission of Millimetre Activity at the Sun (POEMAS) at 45 and 90 GHz, at microwaves from 1 – 15 GHz by the Radio Solar Telescope Network (RSTN), and at high frequencies (212 GHz) by the Solar Submillimetre Telescope (SST). Also, hard X-rays from these flares were simultaneously detected by the Reuven Ramaty High-Energy Solar Spectroscopic Imager (RHESSI). The flux and polarisation radio spectra were fit using a model that simulates gyrosynchrotron emission in a spatially-varying 3D magnetic field loop structure. For the modelling, the magnetic loop geometry was fixed and the field strength was the only free parameter of the magnetic field. In addition, a uniform electron distribution was assumed by the model, with the number density of energetic electrons and the electron spectral index as free parameters. The fitted model reproduced reasonably well the observed degree of polarisation and radio flux spectra for each event yielding the physical parameters of the loop and flaring sources. Our results indicate that the high degree of polarisation during a solar flare can be explained by two sources located at the footpoints of highly asymmetric magnetic loops whereas low polarisation degrees arise from footpoint sources of symmetric magnetic loops.

Keywords Flares · Circular polarisation · Millimetre wavelengths · Magnetic fields

1. Introduction

Solar flares are rapid and intense brightness variations of solar emission at all bands of the electromagnetic spectrum. It is believed that the energy released during these events is of magnetic origin and occurs within active regions of the solar atmosphere, more likely at

✉ D.F. Silva
douglas93f@gmail.com

1 Center for Radio Astronomy and Astrophysics Mackenzie (CRAAM), School of Engineering, Mackenzie Presbyterian University, São Paulo, Brazil

2 SUPA School of Physics and Astronomy, University of Glasgow, G12 8QQ, Glasgow, UK

the top of magnetic loops. The energy released due to magnetic reconnection promotes the acceleration of particles, radiation, and heating of the plasma. A fraction of these accelerated particles is injected into the magnetic loop towards the lower atmosphere (Fletcher et al., 2011), whereas the remaining particles travel in the opposite direction, towards the interplanetary medium, producing type III radio emission (Reid and Ratcliffe, 2014). The charged particles injected downwards into the magnetic loop exhibit a gyration depending on the direction of the magnetic field, producing polarised gyrosynchrotron radiation (Ramaty, 1969).

The microwave emission produced during a solar flare can be expressed as a linear combination of ordinary (O) and extraordinary (X) wave modes. In the optically thin region, the polarisation direction corresponds to the X mode, whereas in the optically thick region to the ordinary mode (Ramaty, 1969). The polarisation in these two modes are opposite in direction and tend to be circular (Gary and Keller, 2004). Thus each polarity is associated with different legs of asymmetric magnetic loops (Énomé, Kakinuma, and Tanaka, 1969; Kundu and Vlahos, 1979; Kundu et al., 2001, 2009; Simões et al., 2013).

Clues of this expected asymmetry of magnetic loops have also been obtained from X-ray observations. Sakao (1994), using data from Yohkoh's Hard X-ray Telescope (HXT), observed an asymmetry in intensity and size of hard X-ray (HXR) sources, with the source at a region of stronger magnetic field producing fewer X-rays, in about 75% of his sample of events. Sakao's interpretation was that at the footpoint with weaker magnetic field there is greater electron precipitation. This is due to the smaller convergence of the field lines, which allowed more electrons to reach the chromosphere and thus generated more X-rays. Similar studies were performed by Goff et al. (2004) and Yang et al. (2012). Their results are in agreement with Sakao's, with about 44% and 75% of their respective samples showing stronger HXR emission from regions with weaker magnetic field intensity, as measured by the Michelson Doppler Imager (MDI, Scherrer et al., 2012). In the radio domain, Kundu et al. (1995) used 17 GHz data to investigate the existence of magnetic asymmetries in magnetic loops. The authors found that the source of intense hard X-rays was associated with unpolarised radio source, whereas the stronger source of radio emission was located over the region with stronger magnetic fields and was also polarised.

Microwave observations from flares are currently one of the best methods to infer the coronal magnetic field in flaring regions, when done in conjunction with models for the gyrosynchrotron emission (Costa and Rosal, 2005; Ramaty et al., 1994; Hurford, Stahli, and Gary, 1989; Fleishman et al., 2020). This method has also been successfully applied to estimate the magnetic field of coronal mass ejections (Bain et al., 2014; Carley et al., 2017). The usual limitation of this method is that it provides only an effective intensity of the magnetic field of the emitting region and it is mostly imposed by the assumed geometry of the model. Several 2D and 3D loop models have been developed in the past decades, with increasing levels of spatial and spectral resolution (Klein and Trottet, 1984; Alissandrakis and Preka-Papadema, 1984; Simões and Costa, 2006; Kuznetsov, Nita, and Fleishman, 2011; Osborne and Simões, 2019; Kuroda et al., 2018; Fleishman et al., 2018) and applied to help in the interpretation of microwave flare data (e.g. Simões and Costa, 2010; Mossessian and Fleishman, 2012; Reznikova, Antolin, and Van Doorsselaere, 2014; Nita et al., 2015; Morgachev et al., 2015; Gordovskyy, Browning, and Kontar, 2017; Cuambe, Costa, and Simões, 2018; Gordovskyy, Browning, and Pinto, 2019).

In the last decade, with the increase in computing power, improvements in the gyrosynchrotron emission algorithms, availability of routines for measurements of the photospheric magnetic vector, as well as codes for coronal magnetic field reconstruction, it is now possible to use 3D loop models in the calculation of the gyrosynchrotron emission from flares, and

thus allow the investigation of asymmetries in magnetic loops (e.g. Fleishman et al., 2016). Despite several studies showing the importance of the optically thick part of the microwave spectrum (Bastian, Benz, and Gary, 1998; Fleishman and Melnikov, 2003; Shevgaonkar and Kundu, 1985), source opacity and projection effects make the interpretation of optically thick emission difficult (e.g. Simões and Costa, 2006). Nevertheless, given the typical source conditions, the millimetric emission is expected to be optically thin, thus providing a more direct view into the properties of the accelerated electrons and the magnetic field of the source.

Observations of flare in the millimetric range are still less common than observations in the centimetric range. In the past 30 years, flare observations have been made with the Berkeley-Illinois-Maryland Array (BIMA Kundu et al., 1991; Silva et al., 1996; Kundu et al., 2000), the Köln Observatory for Submillimeter and Millimeter Astronomy (KOSMA, e.g. Lüthi, Magun, and Miller, 2004), and the Submillimeter Solar Telescope (SST, Kaufmann et al., 1994; Raulin et al., 1999, 2004; Giménez de Castro et al., 2009, 2013), with the latter still in operation.

From November 2011 through the end of 2013, the POlarisation Emission of Millimetre Activity at the Sun (POEMAS, Valio et al., 2013) telescopes observed the Sun at 45 and 90 GHz in both right and left circular polarisation, with a high temporal cadence of 10 ms. During this observing period, several flares were detected; Hidalgo Ramírez et al. (2019) investigated centre-to-limb effects on the flux density and polarisation of the millimetric emission, finding a correlation between the heliocentric position and the polarisation degree in a sample of 30 events.

We present an analysis of two solar flares (SOL2013-02-17T15:51 and SOL2013-11-05T18:13) observed with POEMAS to study their magnetic field configuration, in particular, the magnetic asymmetry of the footpoints of the flaring loops. We employed different observational datasets, described in Section 2, to constrain many of the free parameters of the model, which was then used to fit the flaring spectral data. The characteristics of the magnetic field were inferred from a model developed by Simões (2009), which calculates the gyrosynchrotron radiation in a spatially-varying magnetic field 3D loop, described in Section 3. Our strategy was to use the observed polarisation degree observed by POEMAS to restrict the model fit to infer the magnetic field asymmetry during the flares. The results, discussion, and conclusions of this work are detailed in Sections 4, 5, and 6, respectively.

2. Observational Data

In this work, we investigated two solar flares, SOL2013-02-17T15:51, an M1.9 GOES class event, and SOL2013-11-05T18:13, an M1.0 GOES class event. Both flares were observed at 45 and 90 GHz, in left- and right-handed circular polarisation by POEMAS. The calibration method to obtain the flux density at 45 and 90 GHz is described in Valio et al. (2013). We also employed microwave data from the Radio Solar Telescope Network (RSTN, Guidice, 1979), from the Sagamore Hill Observatory. SOL2013-02-17 was also observed at 212 GHz by Solar Submillimeter Telescope (SST, Kaufmann et al., 1994).

The combined radio observations from 5 to 212 GHz (RSTN, POEMAS, and SST) were used to build the radio flare spectra for our analysis. Using POEMAS's flux density of the left (L) and right (R) circular polarisation channels at 45 and 90 GHz we obtained the degree of polarisation, defined as

$$p = \frac{R - L}{R + L}. \tag{1}$$

Since these radio observations have no spatial resolution, to obtain information about the loop configuration and position where these sources are located we rely on ultraviolet (UV) images from the Atmospheric Imaging Assembly (AIA, Lemen et al., 2012), on board of the Solar Dynamics Observatory (SDO, Pesnell, Thompson, and Chamberlin, 2012). To locate the footpoints of the flaring loops, we employed the hard X-ray (HXR) imaging capabilities of the Reuven Ramaty High Energy Spectroscopic Imager (RHESSI, Lin et al., 2004). RHESSI HXR images were constructed using CLEAN (Hurford et al., 2002) with front detectors 2 to 8, with a beam width factor of 1.5 (e.g. Simões and Kontar, 2013). All SDO/AIA and RHESSI images were taken near the peak time of the impulsive phase of the flares, however avoiding saturated AIA images. Moreover, photospheric magnetograms from SDO's Helioseismic and Magnetic Imager (HMI, Scherrer et al., 2012) were used to estimate the highest magnetic field values at the flaring regions. All this information was used to constrain the magnetic field model of our 3D flaring loops.

2.1. SOL2013-02-17

SOL2013-02-17T15:51, a GOES class M1.9 event, occurred at the NOAA active region 11675 (N12E17). The time profiles of the event are shown in Figure 1: GOES soft X-ray channels 1 – 8 and 0.5 – 4 Å (1a), Fermi Gamma-ray Burst Monitor (GBP, Meegan et al., 2009) HXR count rates at selected energy bands 25 – 50, 50 – 100, and 100-300 keV (1b), POEMAS 45 and 90 GHz flux (1c) and polarisation degree (1d). The peak of the soft X-rays occurs later at 15:51 UT. The HXR and POEMAS lightcurves show a typical impulsive burst, occurring during the rising phase of the SXR emission. We defined the time for our analysis at the peak of the 90 GHz emission (15:47:22 UT, indicated by the vertical line in Figure 1) to have a better signal-to-noise ratio for the spectra and polarisation data. The polarisation degree p at 45 and 90 GHz (Figure 1d) indicates that this event is only weakly polarised, with p below $+0.1$ (right-handed circular polarisation) at both frequencies, during the impulsive phase.

RHESSI HXR 50 – 100 keV intensity contours, highlighting the location of the main flare footpoints, have asymmetric intensities and both are well associated with the flare ribbons seen in UV SDO/AIA 1700 Å image (Figure 2b). The UV ribbons and HXR footpoints are located at opposite sides of the magnetic neutral line as depicted by the SDO/HMI line-of-sight (LOS) magnetogram of the flaring region taken near the peak time of the flare (Figure 2b).

2.2. SOL2013-11-05

The flare SOL2013-11-05T18:13, a GOES class M1.0 event, occurred between 18:08:00 and 18:17:00 UT in NOAA active region 1890 (S12E47). Similarly to the previous event, the lightcurves for GOES SXR channels, Fermi/GBM HXR counts, POEMAS 45 and 90 GHz flux density and polarisation degree are shown in Figure 3. This event also has a typical impulsive behaviour, although it displays a slower rise in emission before the more impulsive peak seen at HXR and millimetric emission. The polarisation at 45 and 90 GHz was predominant in the L sense, with values around -0.4 at 45 GHz and -0.2 at 90 GHz during the impulsive phase (see Figure 3d).

The flare ribbons observed near the peak of the impulsive phase at 1600 Å by SDO/AIA are depicted in Figure 4a. The ribbons are well associated with the HXR 100 – 300 keV footpoints, indicated by the contours of the reconstructed RHESSI CLEAN image. The HXR footpoints and UV ribbons lie at opposite sides of the magnetic neutral line, revealed by the SDO/HMI LOS magnetic field shown in Figure 4b.

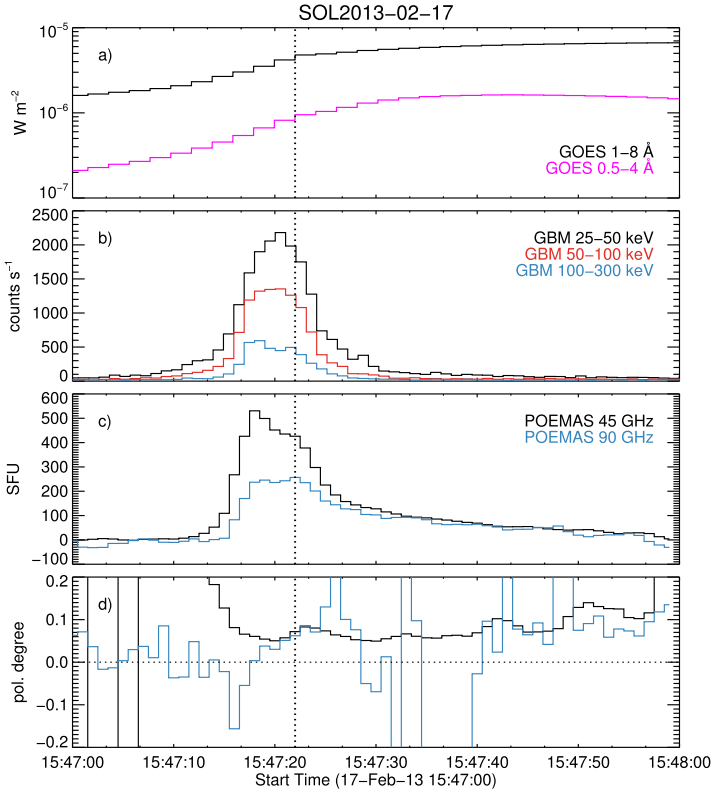

Figure 1 Lightcurves of SOL2013-02-17. (**a**) GOES SXR flux at 1 – 8 and 0.5 – 4 Å, (**b**) HXR count rate from Fermi/GBM at 25 – 50, 50 – 100, 100 – 300 keV energy bands, (**c**) POEMAS 45 and 90 GHz flux density, and (**d**) polarisation degree. The vertical lines in all panels indicate the peak time of the 90 GHz emission, 15:47:22 UT, chosen for the analysis.

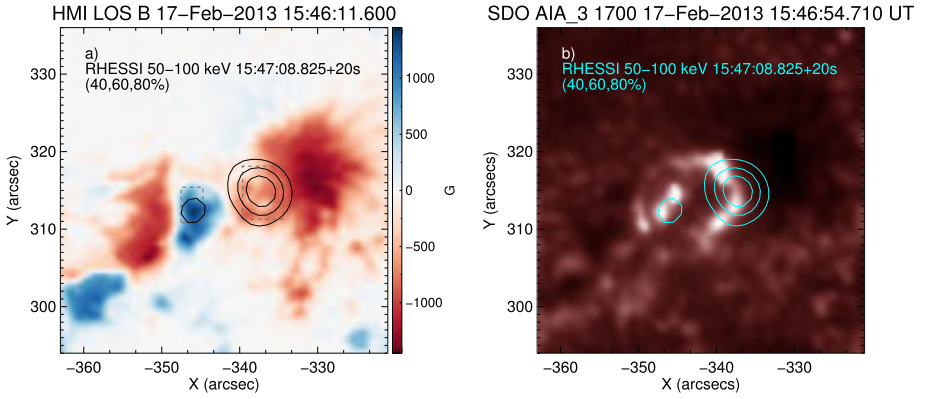

Figure 2 (**a**) SDO/HMI line-of-sight (LOS) magnetogram of the flaring region taken near the peak time of the flare SOL2013-02-17T15:51, overlaid with RHESSI HXR 50 – 100 keV contours. (**b**) SDO/AIA 1700 Å image showing the bright flare ribbons near the peak of the impulsive phase of the flare overlaid by RHESSI HXR 50 – 100 keV intensity contours at 40%, 60% and 80%.

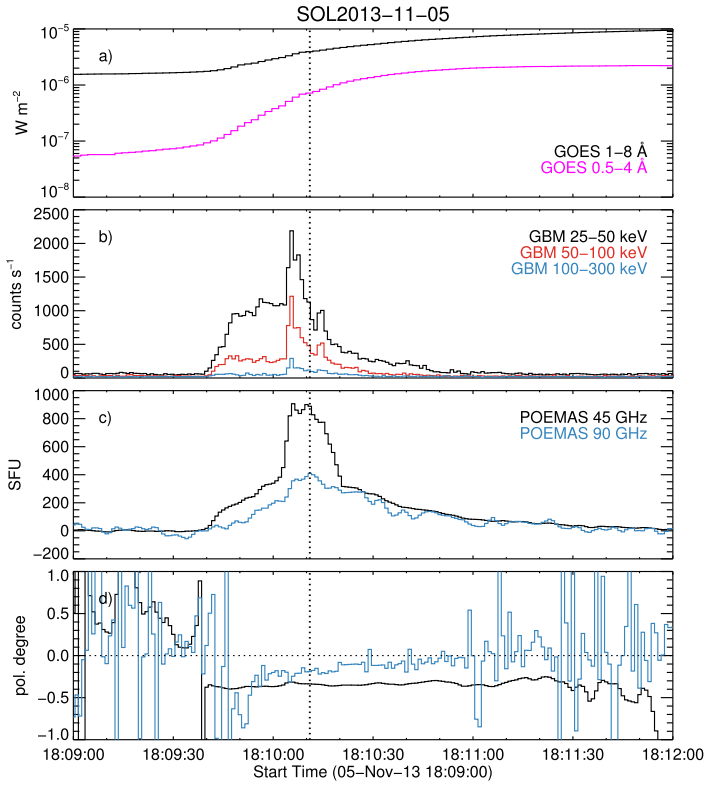

Figure 3 Lightcurves of SOL2013-11-05. (**a**) GOES SXR flux at 1 – 8 and 0.5 – 4 Å, (**b**) HXR count rate from Fermi/GBM at 25 – 50, 50 – 100, 100 – 300 keV energy bands; (**c**) POEMAS 45 and 90 GHz flux density and (**d**) polarisation degree. The vertical lines in all panels indicate the peak time of the 90 GHz emission, 18:10:10 UT, chosen for the analysis.

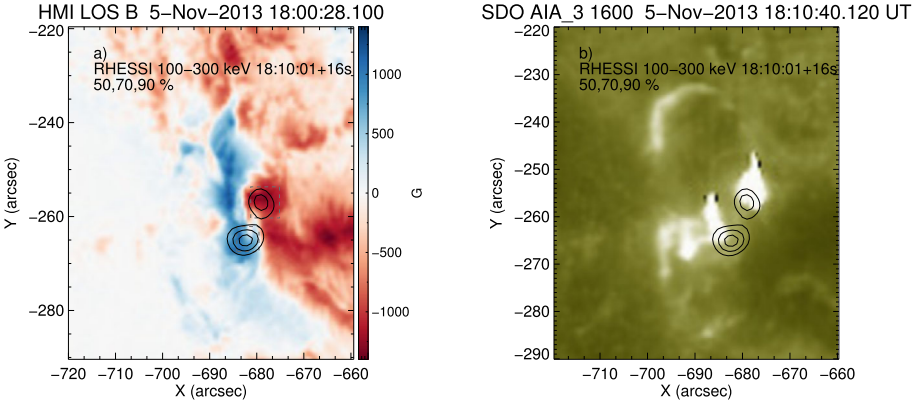

Figure 4 (**a**) SDO/HMI LOS magnetogram of the flaring region taken near the peak time of the flare SOL2013-11-05, overlaid with RHESSI HXR 50 – 100 keV contours. (**b**) SDO/AIA 1600 Å image showing the bright flare ribbons near the peak of the impulsive phase of the flare overlaid by RHESSI HXR 100 – 300 keV intensity contours at 50%, 70% and 90%.

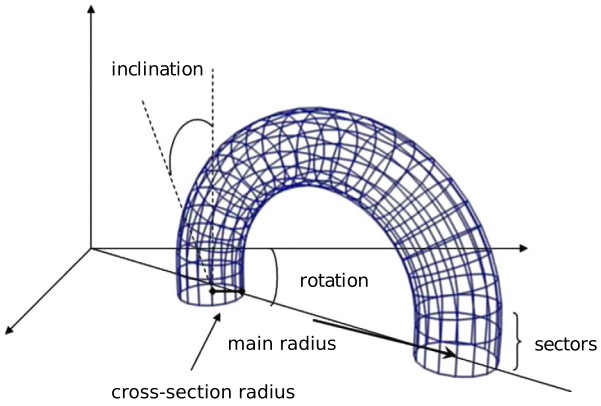

Figure 5 Geometry of the magnetic loop showing the parameters used in the model *gyro3D* (Simões, 2009).

3. Description of the Model

We employed the model developed by Simões (2009), *gyro3D*[1] to construct a 3D loop model with an approximate geometry and location of each solar flare on the solar disk. This model was then fit the microwave spectrum and the polarisation degree at 45 and 90 GHz. The model simulates one single 3D semi-circular loop described by its length L_C and cross-section radius r to represent a flaring source. The orientation of the loop with respect to the observer is defined by its heliographic latitude Θ and longitude Φ, rotation angle relative to the solar equator θ_r, and inclination angle with respect to the local vertical θ_i, as indicated in Figure 5. The loop is divided into N uniform sections along its length. Each section is then associated with the parameters, as functions of the loop length z, to describe the magnetic field $B(z)$, temperature T and density $n(z)$ of the thermal plasma and the distribution $f(E, \phi, z)$ of accelerated electrons (as a function of energy E and pitch-angle ϕ) necessary to calculate the gyrosynchrotron emissivity $j_\nu(z)$ and self-absorption $\kappa_\nu(z)$ coefficients. Here, the non-thermal electron population is assumed to have a power-law distribution in energy:

$$f(\mathrm{E}) = \mathrm{E}_{\mathrm{min}}^{\delta-1}\ (\delta - 1)\ \mathrm{N_e}\ \mathrm{E}^{-\delta} \tag{2}$$

with a spectral index δ, normalised to the total electron density N_e above a minimum energy cutoff E_{min}. We also assume an isotropic pitch-angle distribution and uniform distribution of non-thermal electrons along the magnetic loop.

The core program *gyro*[2] used to calculate these coefficients, following Ramaty (1969), is the same program used by Cuambe, Costa, and Simões (2018), and also implemented by Osborne and Simões (2019). We refer to the latter for a complete description of the computational procedures used in the program to obtain $j_\nu(z)$ and $\kappa_\nu(z)$. These coefficients are obtained for both ordinary and extraordinary wave modes, following Ramaty (1969). The radiative transfer of the gyrosynchrotron radiation across the 3D source is calculated following the approach described in Simões and Costa (2006), where each section of the loop is considered a homogeneous region, and therefore the integral of the specific intensity I_ν along the direction of propagation can be reduced to a sum. This calculation results in specific intensity I_ν maps at any chosen frequency, for the ordinary I_+ and extraordinary I_-

[1] Available at https://github.com/pjasimoes/gyro3d.

[2] Available at https://github.com/pjasimoes/gyro.

modes. The total flux density F_ν (in solar flux units, 1 sfu $= 10^{-22}$ W m^{-2} Hz^{-1}) is obtained by summing the flux density of all pixels in the image, for both modes, taking into account the solid angle of the pixels. The gyrosynchrotron theory is based on moderately relativistic electrons with large Faraday rotation. In this case, the radiative transport equation decouples into I_+ and I_- (Ramaty, 1969). The polarisation degree p obtained by Klein and Trottet (1984) is given by

$$p = \text{sign}(\cos\theta)\frac{I_+ - I_-}{I_+ + I_-}. \tag{3}$$

As the millimetre emission originates from moderately relativistic electrons (Kundu et al., 1995), this equation is valid in this frequency range. The calculations are performed from the reference frame of the electromagnetic waves, such that the extraordinary mode has right-handed polarisation and the ordinary mode left-handed, for a positive B. As discussed in Osborne and Simões (2019), in the reference frame of an observer, the polarisation is reversed, therefore $p_{\text{wave}} = -p_{\text{obs}}$. Our polarisation results are presented in the observer's frame.

To keep the number of free parameters for the model fitting to a minimum, we have fixed the following parameters, based on constraints from the observational data and simple assumptions: magnetic loop length, L_C, based on the HXR footpoint separation; inclination angle relative to the local vertical θ_i; temperature T and density $n(z)$ of the thermal plasma, since these parameters affect the free–free emission and Razin suppression effect, and are negligible in the millimetric range; and minimum and maximum energy cutoffs of the accelerated electron distribution, E_{min} and E_{max} respectively. These values of the fixed parameters are listed in Table 1. Other parameters of the flares such as source heliographic position and loop size (L_C), which vary for each flare, were inferred from the UV and HXR images, and are also listed in Table 1. These parameters were the heliographic coordinates (longitude and latitude) and azimuth angle, or the viewing angle with respect to the solar equator.

After fixing some of the input parameters, based on the observations or reasonable assumptions, we are left with the following free parameters:

i) Magnetic field strength along the loop $B(z)$, defined by the magnetic field intensity at the top of the loop B_0 and the mirroring rate at each footpoint σ, according to the following quadratic expression (Kovalev and Korolev, 1976):

$$B(z) = B_0\left[1 + (\sigma - 1)\frac{z^2}{L_c^2}\right], \tag{4}$$

ii) Spectral index δ, and,
iii) Total electron density N_e.

Note that once the magnetic field at the looptop, B_0, and the mirror ratios σ_1 and σ_2 are determined, we can estimate the magnetic field at each footpoint: $B_+ = \sigma_+ B_0$ and $B_- = \sigma_- B_0$ for the positive and negative footpoints of the magnetic loop, respectively.

To obtain the initial guess of the model parameters, we first use the *amoeba* function from Interactive Data Language (IDL), which performs the minimisation of the residual between observed data and model using the downhill simplex method.

As there is a high dependence on the magnetic field asymmetry on the result of the degree of polarisation it was necessary to obtain the uncertainty of this parameter. Thus the Markov Chain Monte Carlo (MCMC) method was used to achieve parameter uncertainties as well as

Table 1 Fixed input parameters to the model.

Parameter	SOL-2013-02-17	SOL2013-11-05
Heliographic latitude Θ (deg)	18	−16
Heliographic longitude Φ (deg)	−22	−49
Loop length (L_C) (10^9 cm)	1	3
Cross-section radius r (10^8 cm)	1.8	1.1
Inclination angle θ_i (deg)	0	0
Rotation θ_r (deg)	5	−135
Thermal electron density n (10^{10} cm^{-3})	1	1
Thermal electron temperature T (MK)	10	10
Minimum energy cutoff $E_{\rm min}$ (keV)	10	10
Maximum energy cutoff $E_{\rm max}$ (MeV)	20	20

Table 2 Range of variation of free parameters for the model fit.

Parameters	SOL2013-02-17	SOL2013-11-05
Loop top magnetic field B_0 (G)	50– 110	50– 145
Mirror rate 1 σ_1	1.0–14	1.0–14
Mirror rate 2 σ_2	1.0–14	1.0–14
Non-thermal electron density N_e 10^7 cm^{-3}	1–100	(0.1–200)
Spectral index δ	1.0–6.0	1.0–6.0

to explore other parameter sets for minimisation. The minimisation of the free parameters was performed within the range shown in Table 2. We propose a simplified model, with fixed loop geometry, to fit the observed data, which assumes that the electrons injected into the loop are symmetric and the transport along the loop is uniform. Due to the application of this simplified model and its intrinsic limitations, the result of the fit to the observed polarisation and flux spectra is an approximation yielding order of magnitude values of the magnetic field and its asymmetry.

The upper limit for the magnetic field strength at the footpoints was inferred to restrict the upper boundaries of the loop top and the mirroring rates in the feet, displayed in Table 2, were chosen so as to be compatible with the magnetic field observations. The maximum absolute values of the line-of-sight magnetic field at the footpoints were obtained from HXR footpoints, indicated by dotted squares in Figures 2b and 4b. We obtained −1972 G and 1722 G for negative and positive magnetic regions, respectively, for SOL2013-11-05. For SOL2013-02-17, we found −920 G and 1270 G.

The results from the calculation of the emission in a 3D magnetic loop yield the flux density and degree of polarisation spectra and location of the 45 and 90 GHz source. These results are listed in Table 3. Next, we describe the results for each event in detail.

4. Results

The results of the model fits to the flux density spectrum and polarisation degree at the time of the peak 90 GHz emission, for SOL2013-02-17 and SOL2013-11-05 are shown

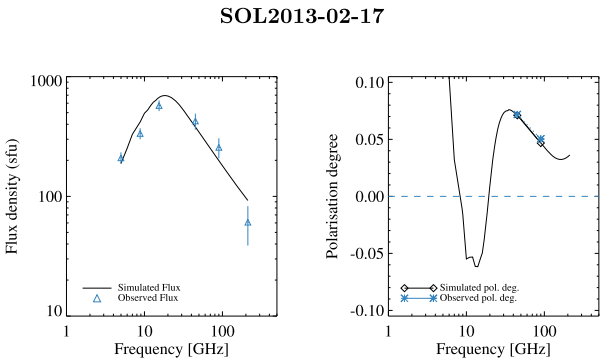

Figure 6 (Left) Radio flux density spectrum at 15:47:22 UT, the peak of the 90 GHz emission of SOL2013-02-17. (Right) 45 and 90 GHz polarisation degree spectrum during the same time interval. The observational data is shown as triangles and our model results shown by the solid line.

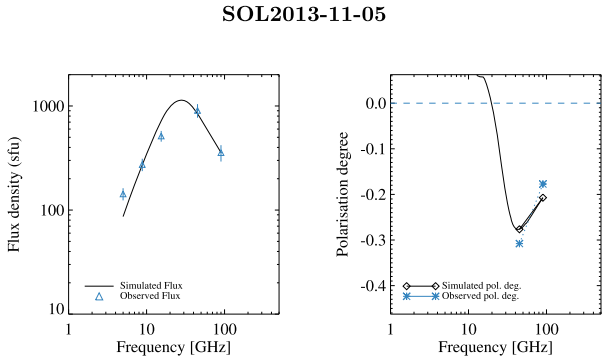

Figure 7 (Left) Radio flux density spectrum at 18:10:10 UT, the peak of the 90 GHz emission of SOL2013-11-05. (Right) 45 and 90 GHz polarisation degree spectrum during the same time interval. The observational data is shown as triangles and our model results shown by the solid line.

in Figures 6 and 7, respectively. The observational data from RSTN, POEMAS, and SST are shown as triangles whereas the model best fit by the solid line. The parameters of the model fit are displayed in Table 3. The model fitting does not match all the data points, as expected, given the limitations and assumptions of our model. It can also be noted that the results of the magnetic field values of both events are lower than those obtained from the magnetogram where the events occurred. Smaller magnetic field values are expected as the lower-frequency than 90 GHz radio sources come typically from higher in the atmosphere.

The calculated 45 GHz brightness temperature maps for SOL2013-02-17 and SOL2013-11-05 are shown in Figure 8 right and left, respectively, overlaid with the corresponding RHESSI HXR contours (the same contours shown in Figures 2 and 4). The loop geometry of our model is represented by the purple line.

As expected, the 45 GHz emission arises from the footpoints where the magnetic field is stronger. Since we assumed a uniform distribution of non-thermal electrons along the loop, the asymmetry in brightness is mostly due to the magnetic field intensity, which affects the amount of emission, and viewing angle that controls the observed polarisation. The calculated 90 GHz maps reveal the same brightness distribution as the 45 GHz maps, and thus are not shown here. Remembering that the fit results of both events were obtained for a fixed magnetic field geometry, where the intensity was the only variable parameter of the magnetic field. Values of the resulting non-thermal electron density and the accelerated electron spectral index despite being somewhat hard, are typical of those found in the literature (e.g. Bastian, Benz, and Gary, 1998).

Table 3 Results from the model calculations.

Parameter	SOL2013-02-17	SOL2013-11-05
Looptop magnetic field B_0 (G)	82 ± 2	80 ± 10
Footpoint magnetic field B_- (G)	-980 ± 30	-1636 ± 20
Footpoint magnetic field B_+ (G)	$+1020 \pm 40$	$+860 \pm 40$
Non-thermal electron density ($10^7 \mathrm{cm}^{-3}$)	1.5 ± 0.1	47 ± 1
Spectral index (δ)	2.3 ± 0.1	2.8 ± 0.2

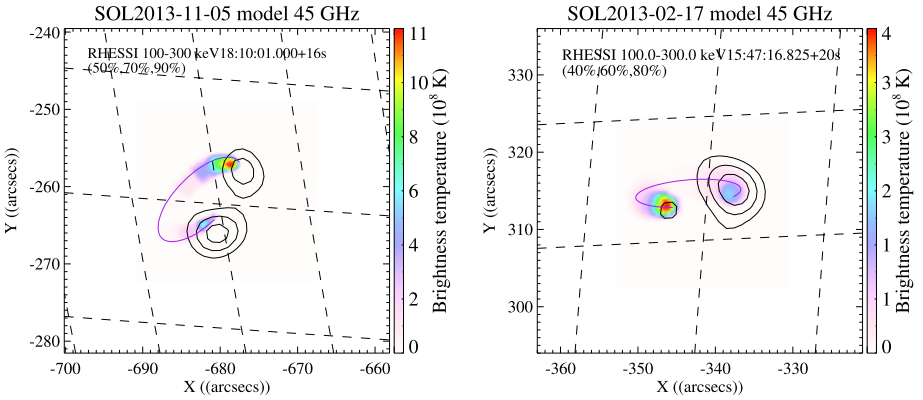

Figure 8 45 GHz brightness temperature maps from the model calculations for (right) SOL2013-02-17 and (left) SOL2013-11-05. RHESSI HXR contours are shown for reference. The solid purple line shows the magnetic loop geometry resulting from our model.

5. Discussion

Sakao (1994) investigated the asymmetry of HXR conjugated footpoints. By using the magnetograms of the flaring regions, he associated the HXR asymmetry with the asymmetry of the magnetic field. The more intense HXR emission originated where the intensity of the magnetic field was weaker, this was observed for four events out of five analysed. The explanation follows from the trap-plus-precipitation models (e.g. Melrose and Brown, 1976) in which footpoints with a weaker magnetic field allow more electrons to precipitate into the denser chromosphere, instead of being magnetically mirrored back to the coronal loops. By comparing HXR and microwave flare images, Kundu et al. (1995) addressed the same issue investigated by Sakao (1994). They found that at the sources with a stronger magnetic field, the radio emission is more intense whereas the HXR source is weaker.

Investigating 32 solar flares observed by Yohkoh, Goff et al. (2004) found that 14 events follow Sakao's results. Yang et al. (2012) analysed about 22 flares detected by RHESSI and found that 75% are similar to that observed by Sakao (1994). Thus, previous authors generally confirm a consistent scenario with asymmetric magnetic mirroring.

Our results for the two flares demonstrated that the most intense radio source, from the fit at both frequencies (45 and 90 GHz), was located at the footpoint with the strongest magnetic field, which also coincided with the emission of the observed weakest hard X-rays source (see Figure 8).

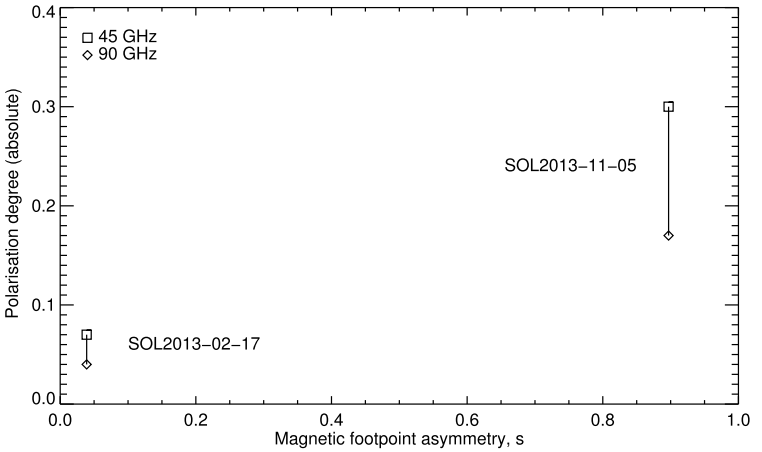

Figure 9 Polarisation degree as a function of the magnetic footpoint asymmetry, given by Equation 5.

To analyse the asymmetry of the magnetic loop, we define the magnetic footpoint asymmetry, s, given by

$$s = \frac{|B_2| - |B_1|}{|B_1|}, \tag{5}$$

where B_2 is the stronger and B_1 the weaker magnetic field intensity of the footpoints. The modeled flaring loop of SOL2013-11-05 presented a footpoint magnetic field difference of about 50%, and hence $s \approx 0.9$. For SOL2013-02-17, the intensity of the footpoints magnetic fields are very similar, giving a magnetic footpoint asymmetry of $s \approx 0.04$. In Figure 9 we show the modelled polarisation degree (absolute value) versus the asymmetry parameter of the magnetic field s. The highly polarised emission for SOL2013-11-05 ($p = 0.2 - 0.3$) originated from a magnetic loop with a large magnetic field asymmetry (see Table 3). For SOL2013-02-17, the weaker polarisation degree ($p = 0.04 - 0.07$) originated from an almost symmetric loop.

It follows from these results, that it might be possible to infer the magnetic footpoint asymmetry even without spatial resolution. However, to confirm these results interferometric radio images are necessary.

However, we cannot rule out the effects of an asymmetric injection of non-thermal electrons in the loop system. Asymmetric reconnection (e.g. Murphy et al., 2012) can potentially lead to asymmetric outflows (Wang et al., 2017, e.g.), which may incur in different acceleration rates of electrons towards the conjugated footpoints. Moreover, the initial pitch-angle distribution of the accelerated electrons (Lee and Gary, 2000) and/or asymmetric injection point (Melnikov, Shibasaki, and Reznikova, 2002; Reznikova et al., 2009) are known to affect their spatial distribution along the magnetic loops and, as a consequence, will affect the polarisation of the observed emission. Although the main physical processes that control the transport of the non-thermal electrons are known (e.g. Hamilton, Lu, and Petrosian, 1990), we lack the sufficient and necessary spatial information about the geometry of the magnetic field in the corona that participates in flaring events. Along with the gyrosynchrotron calculations, electron transport models still have too many parameters that cannot be constrained by observational data, forcing any modelling efforts to rely on a large number of assumptions. However, interferometric images such as the ones produced by ALMA can greatly

improve the diagnostics when combined with the spectrum and temporal variation of each source. Moreover, with spatially resolved images it is possible to deduce the dynamics of the electrons during flares.

6. Conclusions

Here we analysed two flares observed at HXR and several radio wavelengths, with emphasis on the millimetric wave polarisation observed by the POEMAS telescopes. We investigated the solar flares SOL2013-02-17 and SOL2013-11-05, both observed by POEMAS with a good signal-to-noise ratio.

Polarisation measurements by POEMAS at 45 and 90 GHz resulted in degrees of polarisation between 5% and 40% for the events. These events showed opposite sign for the degree of polarisation.

Keeping in mind the limitations of the model, such as a single magnetic loop and the uniform distribution of electrons at each footpoint of the magnetic loop, our main conclusion is that large polarisation degree at millimetre wavelengths from flares originates in highly asymmetric magnetic loops, as seen in the event SOL2013-11-05.

Therefore, an asymmetric magnetic loop simulation in three dimensions is capable of reproducing the observed high polarisation degree of the emitting sources at 45 and 90 GHz. Hence to better understand solar flares, observations not only of the total flux density but also of the polarisation at several radio frequencies are necessary. Of course, spatial resolution also is greatly desired.

Acknowledgements We acknowledge partial financial support from FAPESP (grants 2009/50637 − 0, 2013/24155 − 3, 2013/10559 − 5). We are grateful for the financial support of MACKPESQUISA. P.J.A.S. acknowledges support from the University of Glasgow's Lord Kelvin Adam Smith Leadership Fellowship. The research leading to these results has received funding from the European Community's Seventh Framework Programme (FP7/2007-2013) under grant agreement no. 606862 (F-CHROMA). The authors are grateful to the late Prof. Pierre Kaufmann for the conception insight of the POEMAS telescopes.

Disclosure of Potential Conflicts of Interest The authors declare that they have no conflicts of interest.

References

Alissandrakis, C.E., Preka-Papadema, P.: 1984, Microwave emission and polarization of a flaring loop. *Astron. Astrophys.* **139**(2), 507. ADS.

Bain, H.M., Krucker, S., Saint-Hilaire, P., Raftery, C.L.: 2014, Radio imaging of a type IVM radio burst on the 14th of August 2010. *Astrophys. J.* **782**(1), 43. DOI. ADS.

Bastian, T.S., Benz, A.O., Gary, D.E.: 1998, Radio emission from solar flares. *Annu. Rev. Astron. Astrophys.* **36**, 131. DOI. ADS.

Carley, E.P., Vilmer, N., Simões, P.J.A., Ó Fearraigh, B.: 2017, Estimation of a coronal mass ejection magnetic field strength using radio observations of gyrosynchrotron radiation. *Astron. Astrophys.* **608**, A137. DOI. ADS.

Costa, J.E.R., Rosal, A.C.: 2005, Inference of magnetic fields from solar flares. In: de Gouveia dal Pino, E.M., Lugones, G., Lazarian, A. (eds.) *Magnetic Fields in the Universe: From Laboratory and Stars to Primordial Structures.*, *American Institute of Physics Conference Series* **784**, 544. DOI. ADS.

Cuambe, V.A., Costa, J.E.R., Simões, P.J.A.: 2018, Flare parameters inferred from a 3D loop model data base. *Mon. Not. Roy. Astron. Soc.* **477**(2), 1508. DOI. ADS.

Énomé, S., Kakinuma, T., Tanaka, H.: 1969, High-resolution observations of solar radio bursts with multi-element compound interferometers at 3.75 and 9.4 GHz. *Solar Phys.* **6**, 428. DOI. ADS.
Fleishman, G., Melnikov, V.: 2003, Optically thick gyrosynchrotron emission from anisotropic electron distributions. *Astrophys. J.* **584**, 1071. DOI.
Fleishman, G.D., Xu, Y., Nita, G.N., Gary, D.E.: 2016, Validation of the coronal thick target source model. *Astrophys. J.* **816**(2), 62. DOI. ADS.
Fleishman, G.D., Nita, G.M., Kuroda, N., Jia, S., Tong, K., Wen, R.R., Zhizhuo, Z.: 2018, Revealing the evolution of non-thermal electrons in solar flares using 3D modeling. *Astrophys. J.* **859**(1), 17. DOI. ADS.
Fleishman, G.D., Gary, D.E., Chen, B., Kuroda, N., Yu, S., Nita, G.M.: 2020, Decay of the coronal magnetic field can release sufficient energy to power a solar flare. *Science* **367**(6475), 278. DOI. https://science.sciencemag.org/content/367/6475/278.
Fletcher, L., Dennis, B.R., Hudson, H.S., Krucker, S., Phillips, K., Veronig, A., Battaglia, M., Bone, L., Caspi, A., Chen, Q.: 2011, An observational overview of solar flares. *Space Sci. Rev.* **159**(1-4), 19. DOI. ADS.
Gary, D.E., Keller, C.U. (eds.): 2004, *Solar and Space Weather Radiophysics - Current Status and Future Developments*, *Astrophys. Space Sci. Library* **314**. ADS.
Giménez de Castro, C.G., Trottet, G., Silva-Valio, A., Krucker, S., Costa, J.E.R., Kaufmann, P., Correia, E., Levato, H.: 2009, Submillimeter and X-ray observations of an X class flare. *Astron. Astrophys.* **507**(1), 433. DOI. ADS.
Giménez de Castro, C.G., Cristiani, G.D., Simões, P.J.A., Mandrini, C.H., Correia, E., Kaufmann, P.: 2013, A burst with double radio spectrum observed up to 212 GHz. *Solar Phys.* **284**(2), 541. DOI. ADS.
Goff, C.P., Matthews, S.A., van Driel-Gesztelyi, L., Harra, L.K.: 2004, Relating magnetic field strengths to hard X-ray emission in solar flares. *Astron. Astrophys.* **423**, 363. DOI. ADS.
Gordovskyy, M., Browning, P.K., Kontar, E.P.: 2017, Polarisation of microwave emission from reconnecting twisted coronal loops. *Astron. Astrophys.* **604**, A116. DOI. ADS.
Gordovskyy, M., Browning, P., Pinto, R.F.: 2019, Combining MHD and kinetic modelling of solar flares. *Adv. Space Res.* **63**(4), 1453. DOI. ADS.
Guidice, D.A.: 1979, Sagamore hill radio observatory, air force geophysics laboratory, Hanscom air force base, Massachusetts 01731. Report. In: *Bull. Am. Astron. Soc.* **11**, 311. ADS.
Hamilton, R.J., Lu, E.T., Petrosian, V.: 1990, Numerical solution of the time-dependent kinetic equation for electrons in magnetized plasma. *Astrophys. J.* **354**, 726. DOI. ADS.
Hidalgo Ramírez, R.F., Morosi, A., Silva, D., Simões, P.J.A., Valio, A.: 2019, Center-to-limb variation of solar bursts polarization at millimeter wavelengths. *Solar Phys.* **294**(8), 108. DOI.
Hurford, G.J., Stahli, M., Gary, D.E.: 1989, The secondary spectral component of solar microwave bursts. In: *Bulletin of the American Astronomical Society*, **21**, 836. ADS.
Hurford, G.J., Schmahl, E.J., Schwartz, R.A., Conway, A.J., Aschwanden, M.J., Csillaghy, A., Dennis, B.R., Johns-Krull, C., Krucker, S., Lin, R.P., McTiernan, J., Metcalf, T.R., Sato, J., Smith, D.M.: 2002, The RHESSI imaging concept. *Solar Phys.* **210**, 61. DOI. ADS.
Kaufmann, P., Parada, N.J., Magun, A., Rovira, M., Ghielmetti, H., Levato, H.: 1994, The new solar Submillimeter-Wave Telescope project (SST). In: *Proceedings of Kofu Symposium*, 323. ADS.
Klein, K.-L., Trottet, G.: 1984, Gyrosynchrotron radiation from a source with spatially varying field and density. *Astron. Astrophys.* **141**(1), 67. ADS.
Kovalev, V.A., Korolev, O.S.: 1976, Interpretation of spectra of solar microwave bursts. *Soviet Astron.* **20**, 69. ADS.
Kundu, M.R., Vlahos, L.: 1979, An interpretation of the polarization of microwave bursts. *Astrophys. J.* **232**, 595. DOI. ADS.
Kundu, M.R., White, S.M., Welch, W.J., Bieging, J.H.: 1991, High spatial resolution observations of solar flares at 3.3 mm wavelength. *Adv. Space Res.* **11**(5), 91. DOI. ADS.
Kundu, M.R., Nitta, N., White, S.M., Shibasaki, K., Enome, S., Sakao, T., Kosugi, T., Sakurai, T.: 1995, Microwave and hard X-ray observations of footpoint emission from solar flares. *Astrophys. J.* **454**, 522. DOI. ADS.
Kundu, M.R., White, S.M., Shibasaki, K., Sakurai, T.: 2000, Nonthermal flare emission from MEV-energy electrons at 17, 34, and 86 GHZ. *Astrophys. J.* **545**(2), 1084. DOI. ADS.
Kundu, M.R., Grechnev, V.V., Garaimov, V.I., White, S.M.: 2001, Double loop configuration of a flaring region from microwave, extreme-ultraviolet, and X-ray imaging data. *Astrophys. J.* **563**(1), 389. DOI. ADS.
Kundu, M.R., Grechnev, V.V., White, S.M., Schmahl, E.J., Meshalkina, N.S., Kashapova, L.K.: 2009, High-energy emission from a solar flare in hard X-rays and microwaves. *Solar Phys.* **260**(1), 135. DOI. ADS.
Kuroda, N., Fleishman, G.D., Gary, D.E., Nita, G.M., Chen, B., Yu, S., McTiernan, J.M., White, S.M., Hurford, G.J.: 2018, The observation of 2017-09-09 M1.2 flare by the expanded Owens Valley Solar Array

and the Reuven Ramaty High Energy Solar Spectroscopic Imager. In: *AGU Fall Meeting Abstracts* **2018**, SH14A. ADS.

Kuznetsov, A.A., Nita, G.M., Fleishman, G.D.: 2011, Three-dimensional simulations of gyrosynchrotron emission from mildly anisotropic nonuniform electron distributions in symmetric magnetic loops. *Astrophys. J.* **742**, 87. DOI. ADS.

Lee, J., Gary, D.E.: 2000, Solar microwave bursts and injection pitch-angle distribution of flare electrons. *Astrophys. J.* **543**, 457. DOI. ADS.

Lemen, J.R., Title, A.M., Akin, D.J., Boerner, P.F., Chou, C., Drake, J.F., Duncan, D.W., Edwards, C.G., Friedlaender, F.M., Heyman, G.F., Hurlburt, N.E., Katz, N.L., Kushner, G.D., Levay, M., Lindgren, R.W., Mathur, D.P., McFeaters, E.L., Mitchell, S., Rehse, R.A., Schrijver, C.J., Springer, L.A., Stern, R.A., Tarbell, T.D., Wülser, J.-P., Wolfson, C.J., Yanari, C., Bookbinder, J.A., Cheimets, P.N., Caldwell, D., Deluca, E.E., Gates, R., Golub, L., Park, S., Podgorski, W.A., Bush, R.I., Scherrer, P.H., Gummin, M.A., Smith, P., Auker, G., Jerram, P., Pool, P., Soufli, R., Windt, D.L., Beardsley, S., Clapp, M., Lang, J., Waltham, N.: 2012, The Atmospheric Imaging Assembly (AIA) on the Solar Dynamics Observatory (SDO). *Solar Phys.* **275**, 17. DOI. ADS.

Lin, R.P., Dennis, B., Hurford, G., Smith, D.M., Zehnder, A.: 2004, The Reuven Ramaty high-energy solar spectroscopic imager (RHESSI) mission. In: Fineschi, S., Gummin, M.A. (eds.) *Telescopes and Instrumentation for Solar Astrophysics*, *Society of Photo-Optical Instrumentation Engineers (SPIE) Conference Series* **5171**, 38. DOI. ADS.

Lüthi, T., Magun, A., Miller, M.: 2004, First observation of a solar X-class flare in the submillimeter range with KOSMA. *Astron. Astrophys.* **415**, 1123. DOI. ADS.

Meegan, C., Lichti, G., Bhat, P.N., Bissaldi, E., Briggs, M.S., Connaughton, V., Diehl, R., Fishman, G., Greiner, J., Hoover, A.S., van der Horst, A.J., von Kienlin, A., Kippen, R.M., Kouveliotou, C., McBreen, S., Paciesas, W.S., Preece, R., Steinle, H., Wallace, M.S., Wilson, R.B., Wilson-Hodge, C.: 2009, The Fermi Gamma-Ray Burst Monitor. *Astrophys. J.* **702**(1), 791. http://stacks.iop.org/0004-637X/702/i=1/a=791.

Melnikov, V.F., Shibasaki, K., Reznikova, V.E.: 2002, Loop-top nonthermal microwave source in extended solar flaring loops. *Astrophys. J. Lett.* **580**(2), L185. DOI. ADS.

Melrose, D.B., Brown, J.C.: 1976, Precipitation in trap models for solar hard X-ray bursts. *Mon. Not. Roy. Astron. Soc.* **176**, 15. DOI. ADS.

Morgachev, A.S., Kuznetsov, S.A., Melnikov, V.F., Simões, P.J.A.: 2015, Modeling the distribution of circular polarization degree of microwave emission along the flare loops in event July 19, 2012. *Geomagn. Aeron.* **55**, 1118. DOI. ADS.

Mossessian, G., Fleishman, G.D.: 2012, Modeling of gyrosynchrotron radio emission pulsations produced by magnetohydrodynamic loop oscillations in solar flares. *Astrophys. J.* **748**, 140. DOI. ADS.

Murphy, N.A., Miralles, M.P., Pope, C.L., Raymond, J.C., Winter, H.D., Reeves, K.K., Seaton, D.B., van Ballegooijen, A.A., Lin, J.: 2012, Asymmetric magnetic reconnection in solar flare and coronal mass ejection current sheets. *Astrophys. J.* **751**(1), 56. DOI. ADS.

Nita, G.M., Fleishman, G.D., Kuznetsov, A.A., Kontar, E.P., Gary, D.E.: 2015, Three-dimensional radio and X-ray modeling and data analysis software: revealing flare complexity. *Astrophys. J.* **799**(2), 236. DOI. ADS.

Osborne, C.M.J., Simões, P.J.A.: 2019, Thyr: a volumetric ray-marching tool for simulating microwave emission. *Mon. Not. Roy. Astron. Soc.* **485**(3), 3386. DOI. ADS.

Pesnell, W.D., Thompson, B.J., Chamberlin, P.C.: 2012, The Solar Dynamics Observatory (SDO). *Solar Phys.* **275**(1-2), 3. DOI. ADS.

Ramaty, R.: 1969, Gyrosynchrotron emission and absorption in a magnetoactive plasma. *Astrophys. J.* **158**, 753. DOI.

Ramaty, R., Schwartz, R.A., Enome, S., Nakajima, H.: 1994, *Astrophys. J.* **436**, 941. DOI.

Raulin, J.-P., White, S.M., Kundu, M.R., Silva, A.V.R., Shibasaki, K.: 1999, Multiple components in the millimeter emission of a solar flare. *Astrophys. J.* **522**(1), 547. DOI. ADS.

Raulin, J.P., Makhmutov, V.S., Kaufmann, P., Pacini, A.A., Lüthi, T., Hudson, H.S., Gary, D.E.: 2004, Analysis of the impulsive phase of a solar flare at submillimeter wavelengths. *Solar Phys.* **223**(1-2), 181. DOI. ADS.

Reid, H.A.S., Ratcliffe, H.: 2014, A review of solar type III radio bursts. *Res. Astron. Astrophys.* **14**(7), 773. DOI. ADS.

Reznikova, V.E., Antolin, P., Van Doorsselaere, T.: 2014, Forward modeling of gyrosynchrotron intensity perturbations by sausage modes. *Astrophys. J.* **785**(2), 86. DOI. ADS.

Reznikova, V.E., Melnikov, V.F., Shibasaki, K., Gorbikov, S.P., Pyatakov, N.P., Myagkova, I.N., Ji, H.: 2009, 2002 August 24 limb flare loop: dynamics of microwave brightness distribution. *Astrophys. J.* **697**(1), 735. DOI. ADS.

Sakao, T.: 1994, Characteristics of solar flare hard X-ray sources as revealed with the Hard X-ray Telescope aboard the Yohkoh satellite. PhD thesis, (University of Tokyo), (1994). ADS.

Scherrer, P.H., Schou, J., Bush, R.I., Kosovichev, A.G., Bogart, R.S., Hoeksema, J.T., Liu, Y., Duvall, T.L., Zhao, J., Title, A.M., Schrijver, C.J., Tarbell, T.D., Tomczyk, S.: 2012, The Helioseismic and Magnetic Imager (HMI) investigation for the Solar Dynamics Observatory (SDO). *Solar Phys.* **275**(1-2), 207. DOI. ADS.

Shevgaonkar, R.K., Kundu, M.R.: 1985, Dual frequency observations of solar microwave bursts using the VLA. *Astrophys. J.* **292**, 733. DOI. ADS.

Silva, A.V.R., White, S.M., Lin, R.P., de Pater, I., Shibasaki, K., Hudson, H.S., Kundu, M.R.: 1996, First images of a solar flare at millimeter wavelengths. *Astrophys. J.* **458**, L49. DOI. ADS.

Simões, P.J.d.A.: 2009, Efeitos da distribuição espacial de elétrons na emissão em rádio das explosões solares. PhD thesis, Instituto Nacional de Pesquisas Espaciais, São José dos Campos. http://urlib.net/sid.inpe.br/mtc-m18@80/2009/03.20.18.35.

Simões, P.J.A., Costa, J.E.R.: 2006, Solar bursts gyrosynchrotron emission from three-dimensional sources. *Astron. Astrophys.* **453**(2), 729. DOI. ADS.

Simões, P.J.A., Costa, J.E.R.: 2010, Gyrosynchrotron emission from anisotropic pitch-angle distribution of electrons in 3-D solar flare sources. *Solar Phys.* **266**(1), 109. DOI. ADS.

Simões, P.J.A., Kontar, E.P.: 2013, Implications for electron acceleration and transport from non-thermal electron rates at looptop and footpoint sources in solar flares. *Astron. Astrophys.* **551**, A135. DOI. ADS.

Simões, P.J.A., Fletcher, L., Hudson, H.S., Russell, A.J.B.: 2013, Implosion of coronal loops during the impulsive phase of a solar flare. *Astrophys. J.* **777**(2), 152. DOI. ADS.

Valio, A., Kaufmann, P., Giménez de Castro, C.G., Raulin, J.-P., Fernandes, L.O.T., Marun, A.: 2013, POlarization Emission of Millimeter Activity at the Sun (POEMAS): new circular polarization solar telescopes at two millimeter wavelength ranges. *Solar Phys.* **283**, 651. DOI. ADS.

Wang, J., Simões, P.J.A., Jeffrey, N.L.S., Fletcher, L., Wright, P.J., Hannah, I.G.: 2017, Observations of reconnection flows in a flare on the solar disk. *Astrophys. J.* **847**(1), L1. DOI. ADS.

Yang, Y.-H., Cheng, C.Z., Krucker, S., Hsieh, M.-S., Chen, N.-H.: 2012, Asymmetry of hard X-ray emissions at conjugate footpoints in solar flares. *Astrophys. J.* **756**(1), 42. DOI. ADS.